Hindawi
Advances in Materials Science and Engineering
Volume 2018, Article ID 1939032, 12 pages
https://doi.org/10.1155/2018/1939032

Research Article

Adsorption of Nitrate onto $ZnCl_2$-Modified Coconut Granular Activated Carbon: Kinetics, Characteristics, and Adsorption Dynamics

Lingjie Liu, Min Ji, and Fen Wang

School of Environmental Science and Engineering, Tianjin University, Tianjin 300350, China

Correspondence should be addressed to Fen Wang; wangfen@tju.edu.cn

Received 25 January 2018; Revised 3 April 2018; Accepted 29 April 2018; Published 3 June 2018

Academic Editor: Peter Majewski

Coconut granular activated carbon (CGAC) was modified by impregnating with $ZnCl_2$ solution to remove nitrate from aqueous solutions. Sorption isotherm and kinetic studies were carried out in a series of batch experiments. Nitrate adsorption of both $ZnCl_2$-modified CGAC and CGAC fitted the Langmuir and Freundlich models. Batch adsorption isotherms indicated that the maximum adsorption capacities of $ZnCl_2$-modified CGAC and CGAC were calculated as 14.01 $mgN{\cdot}g^{-1}$ and 0.28 $mgN{\cdot}g^{-1}$, respectively. The kinetic data obtained from batch experiments were well described by pseudo-second-order model. The column study was used to analyze the dynamic adsorption process. The highest bed adsorption capacity of 1.76 $mgN{\cdot}g^{-1}$ was obtained by 50 $mgN{\cdot}L^{-1}$ inlet nitrate concentration, 20 g adsorbents, and 10 $ml{\cdot}min^{-1}$ flow rate. The dynamic adsorption data were fitted well to the Thomas and Yoon–Nelson models with coefficients of correlation $R^2 > 0.834$ at different conditions. Surface characteristics and pore structures of CGAC and $ZnCl_2$-modified CGAC were performed by SEM and EDAX and BET and indicated that $ZnCl_2$ had adhered to the surface of GAC after modified. Zeta potential, Raman spectra, and FTIR suggested the electrostatic attraction between the nitrate ions and positive charge. The results revealed that the mechanism of adsorption nitrate mainly depended on electrostatic attraction almost without any chemical interactions.

1. Introduction

Nitrate is a serious contaminant, which is mainly from agriculture, municipal, and industrial wastewaters [1]. Some conventional techniques are used to remove nitrate from water including biological processes (nitrification, denitrification) [2], zero-valent iron (Fe^0) [3, 4] or magnesium (Mg^0) [5], electrokinetic denitrification [6], reverse osmosis [7], catalytic denitrification [8], ion exchange [9, 10], and chemical reduction [11].

Among several technologies for nitrate removal, adsorption process was widely used because of its convenience, low consumption of energy, and ease of operation. Adsorption, in general, is the removal process of soluble substances that are in solution on a suitable interface [1]. Activated carbon has gained wide attention as an efficient adsorbent which can adsorb various pollutants in aquatic phase especially organic pollutants [12]. However, it shows poor adsorption towards anionic pollutants. As reported in Table 1, most of the papers found in the literature review were devoted to the nitrate adsorption with modified and various synthesis materials.

In addition, studies showed the nitrate adsorption due to the different mechanisms [26–30]. The mechanism of nitrate adsorption by magnetic amine-cross-linked biopolymer includes electrostatic attraction, ion exchange, and surface complex formation [27]. Soybean was modified with calcium chloride and hydrochloric acid and by calcination, and results confirmed that the mechanism of nitrate adsorption was mainly ion exchange [29]. Nitrate was adsorbed by modified biochar (amine-cross-linked reaction that amine group played the main role in nitrate uptake) depending on the electrostatic attraction mechanism [28, 30]. In addition, nitrate was adsorbed by magnetic multiwalled carbon nanotubes depending on the magnetic reaction to the desired separation [26].

Table 1: Literature information on various adsorbents for nitrate removal from water.

Adsorbent	Contact time	q_m (mg·g^{-1})	Reference
Untreated coconut granular activated carbon	2 h	1.7	[13]
$ZnCl_2$-treated coconut granular activated carbon	2 h	10.2	[13]
Commercial activated carbon modified by $C_{13}H_{42}NBr$	120 min	21.51	[12]
Modified anion exchange resin (Dowex 21K XLT) by iron	180 min	333.47	[14]
Modified sugarcane bagasse biochar	60 min	28.21	[15]
Sugar beet bagasse by chemical activation	—	9.14–27.55	[16]
Amine-grafted corn cob/coconut copra	24 h	220.99/261.29	[17]
Pilot-scale-produced wheat/cotton stalk resins	60 min	43.88/33.35	[18]
Lab-scale-produced wheat/cotton stalk resins	60 min	50.24/39.15	[18]
ALR-AE resin	10 min	44.61	[19]
Carbon-silicon nano/bulk composites	60 min	11.343/5.495	[20]
Polyethylene glycol/chitosan	40 min	50.68	[21]
Polyvinyl alcohol/chitosan	40 min	35.03	[21]
Scrap tire chips	3 d	2.92	[22]
Anion exchange resin (Dowex 21K XLT)	180 min	122.23	[14]
New polymeric resin modified with amino and quaternary ammonium groups	24 h	221.8	[23]
Cross-linked organic-inorganic hybrid biocomposites (chitosan/bentonite)	180 min	35.68	[24]
Cross-linked organic-inorganic hybrid biocomposites (chitosan/titanium oxide)	180 min	43.62	[24]
Cross-linked organic-inorganic hybrid biocomposites (chitosan/alumina)	180 min	45.38	[24]
Mg-Al-Cl hydrotalcite-like compound	40 min	19.12	[25]

Although studies have examined nitrate adsorption by modified activated carbon using $ZnCl_2$, little research examined nitrate adsorption mechanisms by modified activated carbon and the adsorption dynamics. Therefore, the main objectives are as follows: (1) nitrate adsorption properties by $ZnCl_2$-modified coconut granular activated carbon ($ZnCl_2$-modified CGAC), including the kinetics and isotherms, in batch experiments; (2) physicochemical properties confirmed by SEM, BET, DFT, zeta potentials, and Raman spectra to fully understand the adsorption mechanisms; and (3) column adsorption experiments with different parameters, including adsorbent bed depth, initial concentration and flow rate, and data analysis from column study using Thomas and Yoon–Nelson models.

2. Materials and Methods

2.1. Materials and Specimen Preparation. Coconut granular activated carbon (CGAC) was gained from Huansheng Company, Henan Province, China. It was sieved through a 2 mm sieve, washed with deionized water, and dried at room temperature for 48 h for future use. CGAC was mixed with $ZnCl_2$ solution. In this study, 200% impregnation ratio was used, which meant that 10 g coconut granular activated carbon was added into the $ZnCl_2$ solution containing 20 g $ZnCl_2$ and 100 ml deionized water. The mixture was stirred for 1 h at 80°C. Then, the sample was dried in an oven for 24 h at 106°C. The resulting sample was placed in the furnace and carbonized at 500°C for 1 h. The product was washed with 0.5 M HCl sequentially and then washed by deionized water repeatedly until the pH of the solution reached about 5.5. After that, the samples were dried at 106°C and stored in a desiccator for further use. All the chemicals including $ZnCl_2$, KNO_3, and HCl were of analytical grade. The nitrate stock solutions (100 mgN·L^{-1}) were prepared by dissolving 0.7218 g KNO_3 in 1000 ml deionized water.

2.2. Batch Experiments. Batch experiments were carried out at different NO_3^--N concentrations (5, 10, 15, 20, 50, 100 mgN·L^{-1}). For adsorption equilibrium studies, experiments were conducted in 500 ml conical flasks containing 2.0 g of adsorbent, 200 ml nitrate solution, and 0.01 M NaCl to keep ion strength at 20°C. The pH was not adjusted during the experiments. The mixtures were shaken at 170 rpm for 12 h and then filtered using a 0.22 μm membrane filter. The concentration of residual NO_3^--N was measured by ion chromatograph (Thermo Scientific Aquion IC 1100). The amount of NO_3^--N adsorbed by per mass unit of adsorbent was calculated by the following equation:

$$q_e = \frac{(C_0 - C_e)V}{W}, \quad (1)$$

where q_e (mgN·g^{-1}) is the adsorbent capacity, C_0 and C_e (mgN·L^{-1}) are the concentrations of NO_3^--N at initial and at equilibrium, respectively, V is the volume of the solution (L), and W is the mass of adsorbent used (g).

For batch kinetic studies, the same procedure was followed, but the aqueous samples were taken at preset time

intervals. The NO_3^--N uptake at any time, q_t (mgN·g^{-1}), was calculated by the following equation:

$$q_t = \frac{(C_0 - C_t)V}{W}, \quad (2)$$

where C_t (mgN·L^{-1}) is the NO_3^--N concentration at any time.

2.3. Characterization. Surface properties of CGAC and $ZnCl_2$-modified CGAC were observed through a scanning electron microscope (SEM) (HITACHI s4800). The distribution of elements on the surface or in the pores of carbon particles was determined by the same SEM together with energy dispersive X-ray spectroscopy.

Pore structure characteristics of CGAC and $ZnCl_2$-modified CGAC were determined by nitrogen adsorption at 77 K (Quantachrome Autosorb iQ2). Prior to gas adsorption measurements, the carbon was degassed at 170°C in a vacuum condition for a period of at least 10 h. The BET surface area was determined by application of the Brunauer–Emmett–Teller (BET) equation [16]. The pore size distributions of the CGAC and $ZnCl_2$-modified CGAC were determined by the density functional theory (DFT) method [16].

Zeta potential measurements of CGAC, $ZnCl_2$-modified CGAC, and nitrate-loaded $ZnCl_2$-modified CGAC were carried out by the microelectrophoresis (Malvern Zetasizer Nano ZS). The samples were grounded in an agate mortar and sieved through a 74 μm sieve. 100 mg of powder samples was mixed with 1 L deionized water by ultrasonic cleaner (KQ-300DE, China) for 10 min at 20°C. After that, the samples were settled for 30 min. The suspension was collected to determine the zeta potential at several pH values from 2.0 to 12.0 using 0.01 M of NaOH and HCl to adjust pH. The pH_{PZC} was the corresponding pH value when the zeta potential was 0 mV.

To make an intensive study on the interaction mechanisms of nitrate onto $ZnCl_2$-modified CGAC, Raman spectroscopic analysis was performed. In the Raman analysis, 0.1 g $ZnCl_2$-modified CGAC was placed in 50 ml of nitrate solution with concentration of 0.5 mol·L^{-1}. The pure solid samples of KNO_3, $ZnCl_2$-modified CGAC, and nitrate-loaded $ZnCl_2$-modified CGAC were analyzed by Raman spectroscopy (DXR Microscope). The laser wavelength used in Raman measurement was 1050 nm.

FTIR spectroscopy (Thermo Nicolet 6700 Spectrometer, USA) was done to identify the chemical functional groups presented on $ZnCl_2$-modified CGAC, nitrate-loaded $ZnCl_2$-modified CGAC, and solid samples of KNO_3. The saturated samples after adsorption were prepared by mixing the $ZnCl_2$-modified CGAC (2 g) with solution (200 ml) containing 500 mgN·L^{-1} of nitrate. Samples of particle size <45 μm were first dried for 24 h at a temperature of 383 K. The dried samples were mixed with finely divided KBr at a ratio of 1 : 100. The spectrum was scanned from 400 to 4000 cm^{-1}.

2.4. Column Studies. In column experiment, a glass column (30 cm height and 2.3 cm inner diameter) was filled with $ZnCl_2$-modified CGAC on glass wool support. In a typical experiment, a synthetic NO_3^--N solution was fed into the column from the top at a desired flow rate using a peristaltic pump. A known quantity of the prepared $ZnCl_2$-modified CGAC was packed in the column to yield the desired bed height of the adsorbent 39 mm, 78 mm, 117 mm (equivalent to 10 g, 20 g, and 30 g of $ZnCl_2$-modified CGAC) at flow rate of 10 ml·min^{-1} and initial NO_3^--N concentration of 20 mgN·L^{-1}. The effect of NO_3^--N concentration on the adsorption capacity was studied using initial NO_3^--N concentrations of 10, 20, and 50 mgN·L^{-1} with column flow rate of 10 ml·min^{-1} and 20 g $ZnCl_2$-modified CGAC. The effect of different flow rates on the adsorption capacity was studied at 5, 10, and 20 ml·min^{-1} with 20 mgN·L^{-1} initial NO_3^--N concentration and 20 g adsorbents. Samples were collected from the bottom of the column at regular time intervals and analyzed for residual nitrate concentrations. The studies were conducted at room temperature (20 ± 2°C), and natural pH of solutions was about 6.5. The flow of the column was continued until the effluent concentration (C_t) approached the influent concentration (C_0), $C_t/C_0 = 0.95$.

The equilibrium NO_3^--N uptake per unit mass of adsorbent (q_0) was calculated by the following equation:

$$V_{\text{total}} = Qt_{\text{total}}. \quad (3)$$

The value of the total mass of NO_3^--N adsorbed, q_{total} (mg), could be calculated from the area under the breakthrough curve:

$$q_{\text{total}} = \int_0^{V_{\text{total}}} (C_0 - C_e)\, dV, \quad (4)$$

where V_{total} is the effluent volume at equilibrium, Q is the volumetric flow rate (ml·min^{-1}), and t_{total} is the total flow time [28, 31].

Equilibrium metal uptake or maximum capacity of the column, q_{eq} (mgN·g^{-1}), in the column was calculated by the following equation:

$$q_{\text{eq}} = \frac{q_{\text{total}}}{m}, \quad (5)$$

where m is the mass of the adsorbent (g).

Total amount of NO_3^--N ion entering column (m_{total}) was calculated by the following equation [32]:

$$m_{\text{total}} = \frac{C_0 Q t_{\text{total}}}{1000}. \quad (6)$$

3. Results and Discussion

3.1. Adsorption Kinetics. The adsorption kinetics described the uptake rate of nitrate ion on the $ZnCl_2$-modified CGAC, which controlled the equilibrium time [33]. The kinetic studies were helpful for predicting the adsorption rate with time and explaining the dynamic interactions of nitrate ions with adsorbents, which gave important information for designing and modeling the processes [27, 33]. The experimental data were fitted by three different kinetic models: the pseudo-first-order model, pseudo-second-order model, and intraparticle diffusion model, and the results were discussed below.

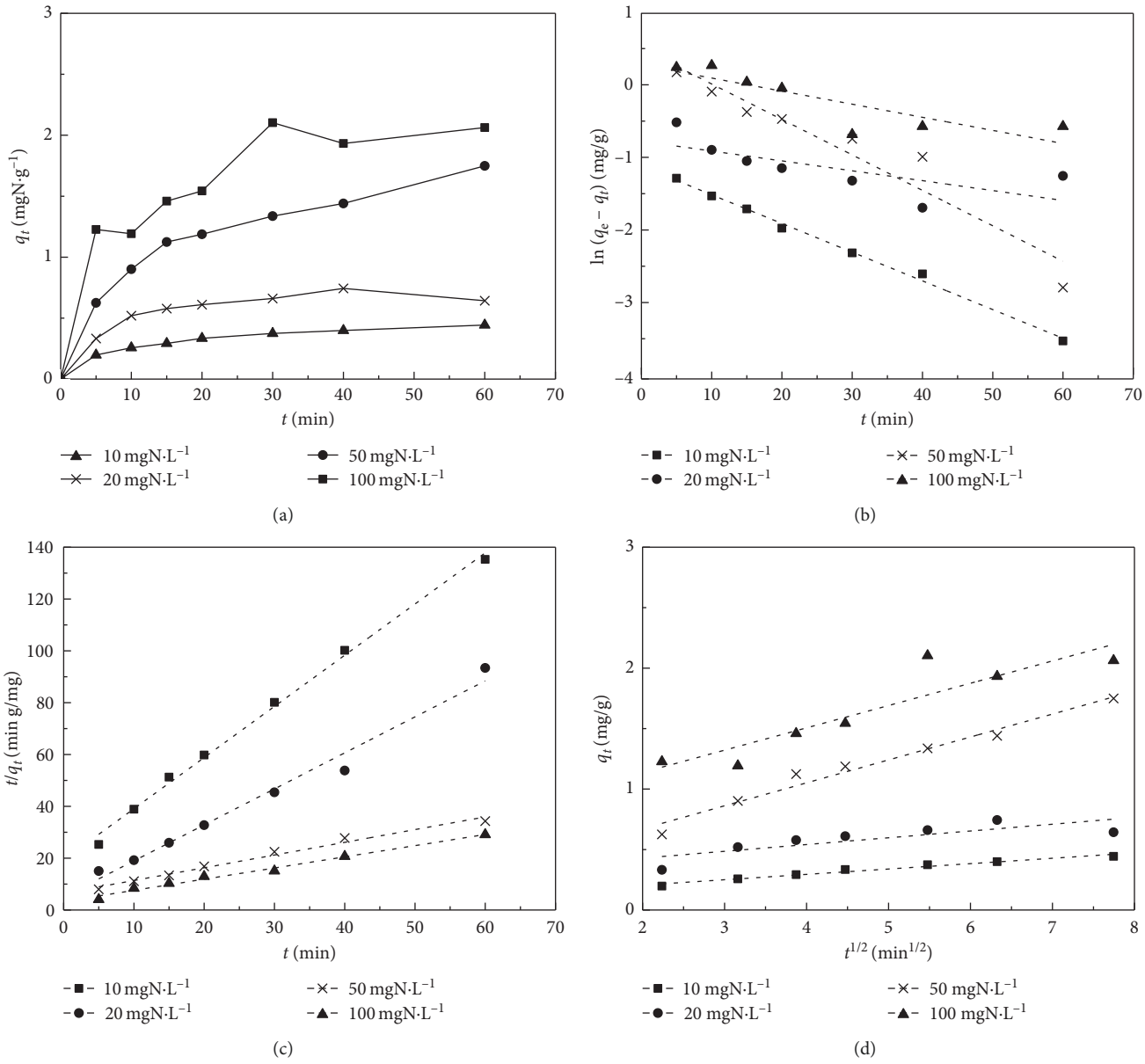

Figure 1: Linear plots of adsorption kinetics: (a) the variation of adsorption capacity with adsorption time at various initial nitrate concentrations; (b) pseudo-first-order adsorption plot; (c) pseudo-second-order adsorption plot; (d) intraparticle diffusion adsorption plot.

The linear equation for pseudo-first-order kinetic model, widely used to predict sorption kinetics, was given by Langergren and Svenska [33], defined as follows:

$$\ln(q_e - q) = \ln q_e - k_1 t. \tag{7}$$

Pseudo-second-order kinetic model, based on equilibrium adsorption, was expressed as follows:

$$\frac{t}{q} = \frac{1}{k_2 q_e^2} + \frac{1}{q_e} t. \tag{8}$$

Intraparticle diffusion model described by Weber and Morris [34] was widely used to explain the rate-limiting step:

$$q_t = k_{dif} \sqrt{t} + C, \tag{9}$$

where q_e and q_t (mg·g^{-1}) are the amount of adsorbate adsorbed at equilibrium and at any time, t (min), respectively, and k_1 (min^{-1}), k_2 (g·mg^{-1}·min^{-1}), and k_{dif} (mgN·(g·min$^{1/2}$)$^{-1}$) were the adsorption rate constant of pseudo-first-order model, pseudo-second-order model, and intraparticular diffusion model, respectively.

The nitrate adsorption by $ZnCl_2$-modified CGAC increased with the increase in initial nitrate concentration as shown in Figure 1(a), and the linear plots of different kinetic models are shown in Figures 1(b)–1(d). Moreover, kinetic constants of different kinetic models for the nitrate adsorption are shown in Table 2.

The correlation coefficients (R^2) for the pseudo-first-order kinetic model, pseudo-second-order kinetic model, and intraparticle diffusion model were 0.413–0.995, 0.977–0.995,

Table 2: Parameters for different adsorption kinetic models.

C_0 (mgN·L^{-1})	$q_{e,exp}$ (mgN·g^{-1})	Pseudo-first-order kinetic model			Pseudo-second-order kinetic model			Intraparticle diffusion model		
		$q_{e,cal}$ (mgN·g^{-1})	k_1 (h^{-1})	R^2	$q_{e,cal}$ (mgN·g^{-1})	k_2 (g·(mgN·h)$^{-1}$)	R^2	k_{dif} (mgN·(g·min$^{1/2}$)$^{-1}$)	c	R^2
10	0.47	0.33	0.040	0.995	0.51	0.202	0.995	0.044	0.117	0.966
20	0.93	0.46	0.014	0.413	0.72	0.380	0.977	0.056	3.175	0.593
50	1.81	1.64	0.049	0.910	2.04	0.037	0.981	0.190	0.293	0.966
100	2.49	1.31	0.018	0.664	2.32	0.057	0.985	0.184	0.769	0.793

and 0.593–0.966, respectively. Meanwhile, according to the calculated value ($q_{e,cal}$) and experimental uptake value ($q_{e,exp}$), the pseudo-second-order model was considered as the best-fit model in describing the nitrate adsorption from aqueous solution [29, 35]. Pseudo-second-order model has been frequently invoked to describe adsorption of inorganic pollutants on GAC-based materials [29], and a similar study reported the nitrate adsorption onto magnetic amine-cross-linked biopolymer fitted with pseudo-second-order model as well [27].

3.2. Adsorption Isotherms. The adsorption isotherm was conducted to determine the maximum adsorption capacities and expressed the relationship between the amount of sorption and residual nitrate concentration at equilibrium [36]. The adsorption isotherm indicated how the adsorption molecules distributed between the liquid phase and the solid phase when the adsorption process reached an equilibrium state [37]. In order to optimize the design of an adsorption system, three adsorption isotherms, namely, the Langmuir, Freundlich, and Temkin isotherm models in their linear forms were applied to the equilibrium data to find the suitable model that could be used for design purpose [37]. Figure 2 typically shows the nitrate adsorption isotherms on the $ZnCl_2$-modified CGAC and CGAC. All the correlation coefficient, R^2 values, and the parameters obtained for the models are summarized in Table 3. The adsorption data fitted satisfactorily to both Langmuir ($R^2 = 0.970$) and Freundlich ($R^2 = 0.982$) models, better than Temkin model ($R^2 = 0.828$), are shown in Table 3 and Figure 2. Application of the Langmuir model for $ZnCl_2$-modified CGAC and CGAC allowed the determination of the maximum equilibrium adsorption capacity [36], which were 14.01 mgN·g^{-1} and 0.28 mgN·g^{-1}, respectively. The nitrate adsorption capacity of modified adsorbents was much higher than that of raw adsorbents. The maximum adsorption capacity obtained for $ZnCl_2$-modified CGAC was higher than the corresponding values assumed by others for polyethylene glycol/chitosan and polyvinyl alcohol/chitosan (11.44 mgN·g^{-1} and 7.91 mgN·g^{-1}) [21]. In addition, the constant $1/n$ in the range of 0-1 showed the favorable conditions for adsorption [38].

3.3. Characteristics

3.3.1. SEM Analysis. The scanning electron microscopy images of CGAC and $ZnCl_2$-modified CGAC are shown in Figures 3(a) and 3(b), respectively. Compared with the surface of CGAC (Figure 3(a)), $ZnCl_2$-modified CGAC had crystal on the surface (Figure 3(b)). The elemental composition of $ZnCl_2$-impregnated activated carbon determined by EDAX is shown in Table 4. After modified by $ZnCl_2$, the carbon content decreased from 74.75% to 37.61% and the zinc contents and the chloride contents increased to 53.61% and 0.49%, respectively.

3.3.2. BET Analysis. The surface area and pore characteristics are shown in Table 5. The BET specific surface area of CGAC was 876.752 m^2·g^{-1}, and the surface area of $ZnCl_2$-modified CGAC decreased to 567.524 m^2·g^{-1}. It was obvious that the pore width decreased after impregnation with $ZnCl_2$, from 0.518 nm to 0.492 nm. The decrease of surface area was ascribed to blockage of pore openings by the $ZnCl_2$ that prohibited access of adsorbing gas molecules [29]. This indicated that the $ZnCl_2$ had adhered to the surface of the CGAC and the result was confirmed by the SEM analysis as shown in Figure 3. It had been proved that activated carbon with large amounts of pore structures was inefficient for adsorption capacity [4, 28, 39]. As a result, micropore adsorption was absent for the potential nitrate adsorption by activated carbon [28].

3.3.3. Zeta Potentials. Zeta potentials of original activated carbon, $ZnCl_2$-modified CGAC, and nitrate-loaded $ZnCl_2$-modified CGAC as a function of pH are shown in Figure 4. All the samples of the zeta potentials became more negative with the increase in pH, probably because of the deposition of more OH^- on the adsorbent surface [40]. Zeta potentials of CGAC were in the range of +12.55 to −30.50 mV as the initial pH of the suspensions increased from 2.01 to 11.99. After modified by $ZnCl_2$, zeta potentials of $ZnCl_2$-modified CGAC increased slightly (+14.60 to −29.65 mV) in designed pH range. Point of zero charge pH (pH_{pzc}) of CGAC was located at 2.39. After the $ZnCl_2$ modification, pH_{pzc} of modified GAC had a slight increase to 2.56. This suggested that $ZnCl_2$ loaded on the surface of activated carbon increased positive charge on activated carbon surface. After adsorption, zeta potentials had an apparent decrease at the pH of 5.3~12, this illustrated that nitrate ions had been adsorbed on the surface of $ZnCl_2$-modified CGAC, and the adsorption mechanism of $ZnCl_2$-modified CGAC for nitrate was based on electrostatic attraction [28].

3.3.4. Raman Spectra. Figure 5 shows the Raman spectra of $ZnCl_2$-modified CGAC, pure KNO_3, and nitrate-loaded

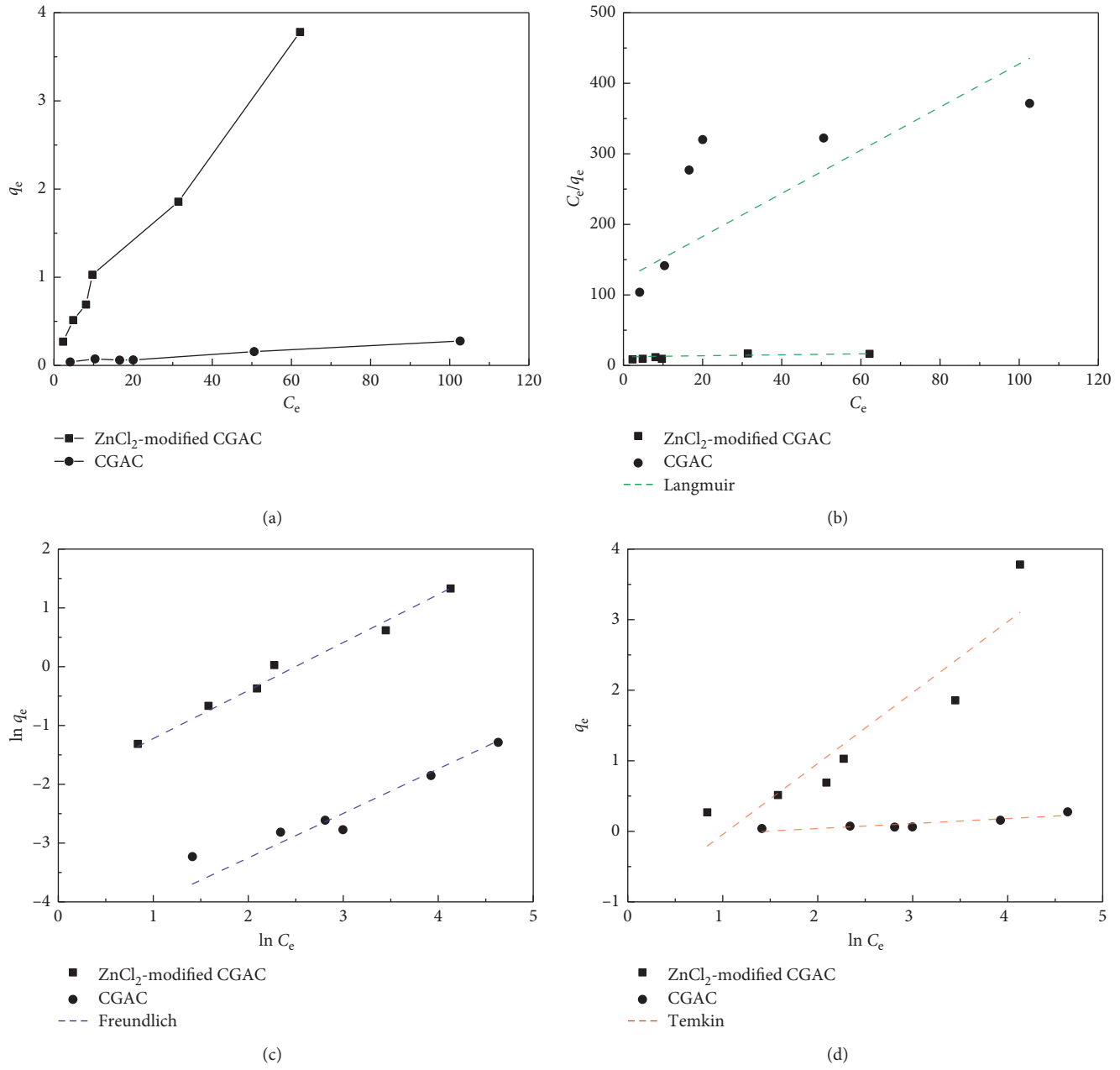

Figure 2: Adsorption isotherms for nitrate adsorption onto CGAC and $ZnCl_2$-modified CGAC: (a) experimental points; (b) Langmuir adsorption isotherm plots; (c) Freundlich adsorption isotherm plots; (d) Temkin adsorption isotherm plots.

Table 3: Langmuir, Freundlich, and Temkin model constants for nitrate adsorption.

Adsorbent	Langmuir $C_e/q_e = (1/QK_L) + (C_e/Q)$			Freundlich $\ln q_e = \ln K_f + (1/n)\ln C_e$			Temkin $q_e = B\ln K_T + B\ln C_e$		
	Q (mgN·g^{-1})	K_L (L·mg^{-1})	R^2	K_f (mgN·g^{-1})·(L·mg^{-1})$^{1/n}$	$1/n$	R^2	K_T (L·mg^{-1})	B (J·mol^{-1})	R^2
$ZnCl_2$-modified CGAC	14.01	0.0058	0.970	0.13	0.813	0.982	0.35	1.0055	0.828
CGAC	0.28	0.0294	0.817	0.00851	0.746	0.962	0.24	0.0707	0.745

C_e is the equilibrium concentration (mg·L^{-1}); Q is the monolayer saturation adsorption capacity; K_L is the Langmuir constant (L·mg^{-1}); K_f is the adsorbent-adsorbate relative affinity in the adsorption process ((mgN·g^{-1})·(L·mg^{-1})$^{1/n}$); K_T is equilibrium blinding constant (L·mg^{-1}); and B is the Temkin constant related to the heat of adsorption.

$ZnCl_2$-modified CGAC. Two peaks at 1332.5 cm^{-1} and 1586.1 cm^{-1} in the Raman spectrum of $ZnCl_2$-modified CGAC were the characteristic peaks of polycrystalline graphites, namely, G (graphite) band and D (disorder) band, which explicitly appear at about 1580 and 1360 cm^{-1}, respectively. The pure KNO_3 crystal had a characteristic

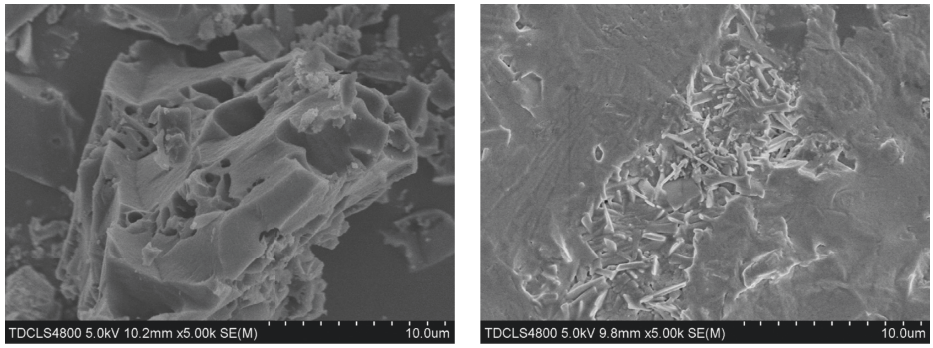

(a) (b)

Figure 3: SEM images of CGAC and $ZnCl_2$-modified CGAC.

Table 4: EDAX data for CGAC and $ZnCl_2$-modified CGAC.

CGAC		$ZnCl_2$-modified CGAC	
Element	Wt.%	Element	Wt.%
C	74.75	C	37.61
O	6.14	O	0.9
Al	3.29	Al	7.38
Mg	15.21	Cl	0.49
Ca	0.61	Zn	53.61

Table 5: Pore characteristics of CGAC and $ZnCl_2$-modified CGAC.

Adsorbent	Surface area ($m^2 \cdot g^{-1}$)	Pore width (nm)	Pore volume ($cm^3 \cdot g^{-1}$)
CGAC	876.752	0.518	0.404
$ZnCl_2$-modified CGAC	567.524	0.492	0.253

peak at 1042.3 cm^{-1}. After the adsorption process, the nitrate on $ZnCl_2$-modified CGAC illustrated the Raman peak at 1039.4 cm^{-1}, which was almost overlapped with the peak of KNO_3. The results indicated that nitrate ions were adsorbed onto the surface of $ZnCl_2$-modified CGAC through electrostatic attraction between the free nitrate ions and the positively charged ions of $ZnCl_2$ sites [28], which corresponded well to the decrease of zeta potentials after nitrate adsorption onto $ZnCl_2$-modified CGAC.

3.3.5. FTIR Spectra. Figure 6 shows the FTIR spectra of $ZnCl_2$-modified CGAC, nitrate-loaded $ZnCl_2$-modified CGAC, and solid KNO_3 samples. The FTIR spectra analysis of these samples illustrated the change of functional groups.

In FTIR spectra of $ZnCl_2$-modified CGAC and nitrate-loaded $ZnCl_2$-modified CGAC, the bands at about 3430 cm^{-1} were ascribable to ν (O-H) vibrations in hydroxyl groups. The low-frequency values for these bands suggested that the hydroxyl groups were involved in hydrogen bonds and the position of the band due to nonbonded OH groups was usually above 3500 cm^{-1} for alcohols, phenols, and carboxylic acids [41]. The O-H stretching vibrations occurred within a broad range of frequencies indicating the presence of "free" hydroxyl groups and bonded O-H bands

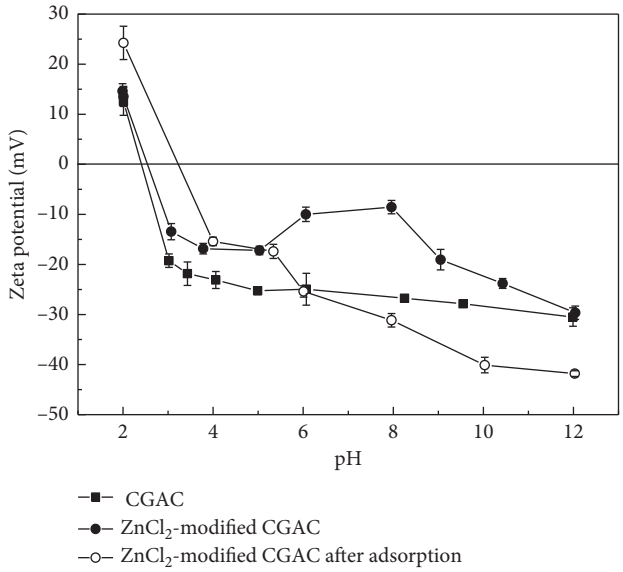

Figure 4: Zeta potentials of CGAC, $ZnCl_2$-modified CGAC, and $ZnCl_2$-modified CGAC after nitrate adsorption.

of carboxylic acids. The bands observed at 1800–1000 cm^{-1} were presumed to be associated with oxygenated C=O and C-O-R structures as the range was reported to reflect the presence of moieties of different C=O (amide, esters, carboxylic acids, quinines, etc.) and C-O-R (aryl and alkyl esters, carboxylic) structures depending on the extent of coalification [42].

Nitrate curve in Figure 6 and the pure KNO_3 crystal had a characteristic peak at 1384.66 cm^{-1} in FTIR spectra. Compared with the curve of $ZnCl_2$-modified CGAC, a new peak at 1384.66 cm^{-1} (NO_3^-) was observed in the curve of nitrate-laden $ZnCl_2$-modified CGAC which was assigned to the special vibration of nitrate. Meanwhile, few special vibrations could be shown in FTIR spectra, so that the main mechanism of adsorption nitrate based on electrostatic attraction almost without any chemical interactions existed.

3.4. Column Studies. To investigate the adsorption ability to the continuous nitrate removal from solution onto

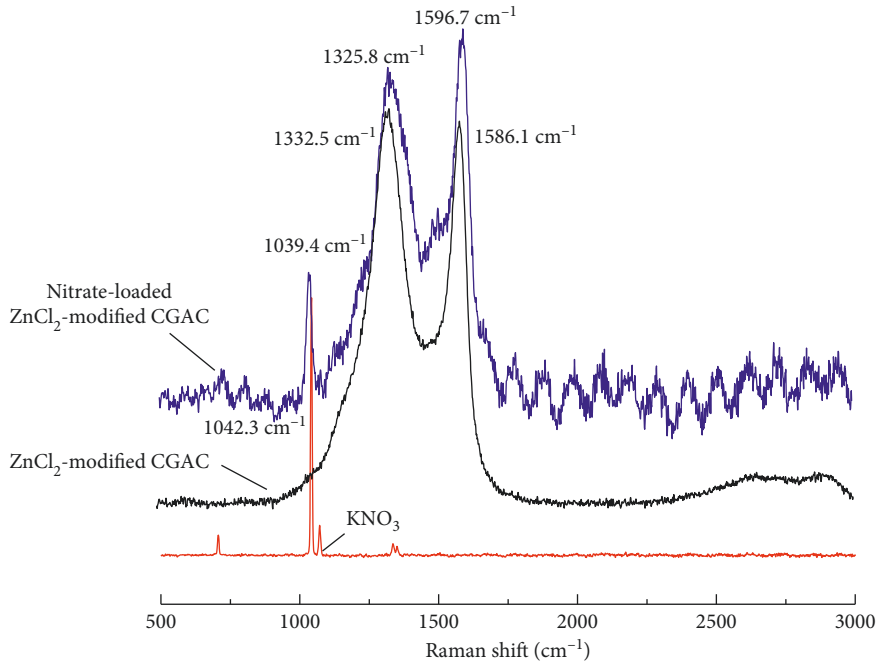

Figure 5: Raman spectra of CGAC, $ZnCl_2$-modified CGAC, and anion-laden $ZnCl_2$-modified CGAC.

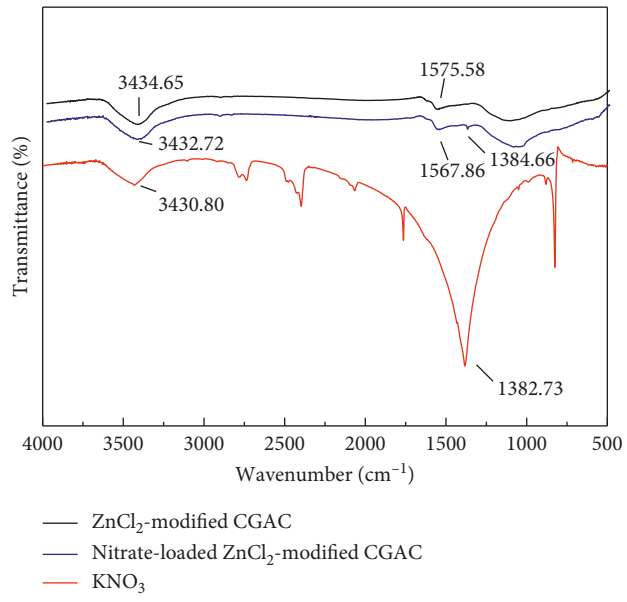

Figure 6: FTIR pattern of $ZnCl_2$-modified CGAC, nitrate-loaded $ZnCl_2$-modified CGAC, and solid KNO_3.

$ZnCl_2$-modified CGAC, dynamic column adsorption tests and the dynamic models were conducted to evaluate the performance of a continuous system.

3.4.1. Effect of the Column Depth on the Breakthrough Curves. As shown in Figure 7(a) and Table 6, when the mass of adsorbent was 10 g, 20 g, and 30 g, the breakthrough points occurred at the time of 200 min, 320 min, and 650 min, respectively. The saturated adsorption capacities of $ZnCl_2$-modified CGAC (10 g, 20 g, and 30 g) in column were about 0.25 mgN·g^{-1}, 0.20 mgN·g^{-1}, and 0.17 mgN·g^{-1}, respectively. The breakthrough time increased with the increase in mass which might be due to the more contact time. The increase in NO_3^--N uptake capacity with the increasing bed depth in the column may be due to increased adsorbent surface area, which provided more binding sites for the column adsorption [43, 44].

3.4.2. Effect of Flow Rates on the Breakthrough Curves. As shown in Figure 7(b) and Table 6, the breakthrough curve generally occurred faster with higher flow rate at 20 ml·min^{-1}. With the increases in flow rate, the adsorption capacities were 0.18 mgN·g^{-1}, 0.20 mgN·g^{-1}, and 0.27 mgN·g^{-1}, respectively. As indicated in Figure 7(b), the breakthrough curve became steeper as the flow rate increased. This was due to that, at a high rate of influent, NO_3^--N did not have enough time to contact with $ZnCl_2$-modified CGAC [43]. At a low rate of influent, NO_3^--N maybe had more time to be in contact with adsorbent [44]. Breakthrough time reaching saturation was increased significantly with a decrease in the flow rate.

3.4.3. Effect of Influent Concentration on the Breakthrough Curves. As shown in Figure 7(c) and Table 6, it is illustrated that the adsorption process reached saturation faster and the breakthrough time decreased with increasing influent NO_3^--N concentration. The adsorption capacities of $ZnCl_2$-modified CGAC for nitrate were 0.12 mgN·g^{-1}, 0.20 mgN·g^{-1}, and 0.26 mgN·g^{-1}, respectively. The maximum capacity at 50 mgN·L^{-1} was higher than those at 10 mgN·L^{-1} and 20 mgN·L^{-1}. This might be attributed to high influent NO_3^--N concentration providing higher driving force for the transfer process to overcome the mass transfer resistance [45]. This result indicated that the

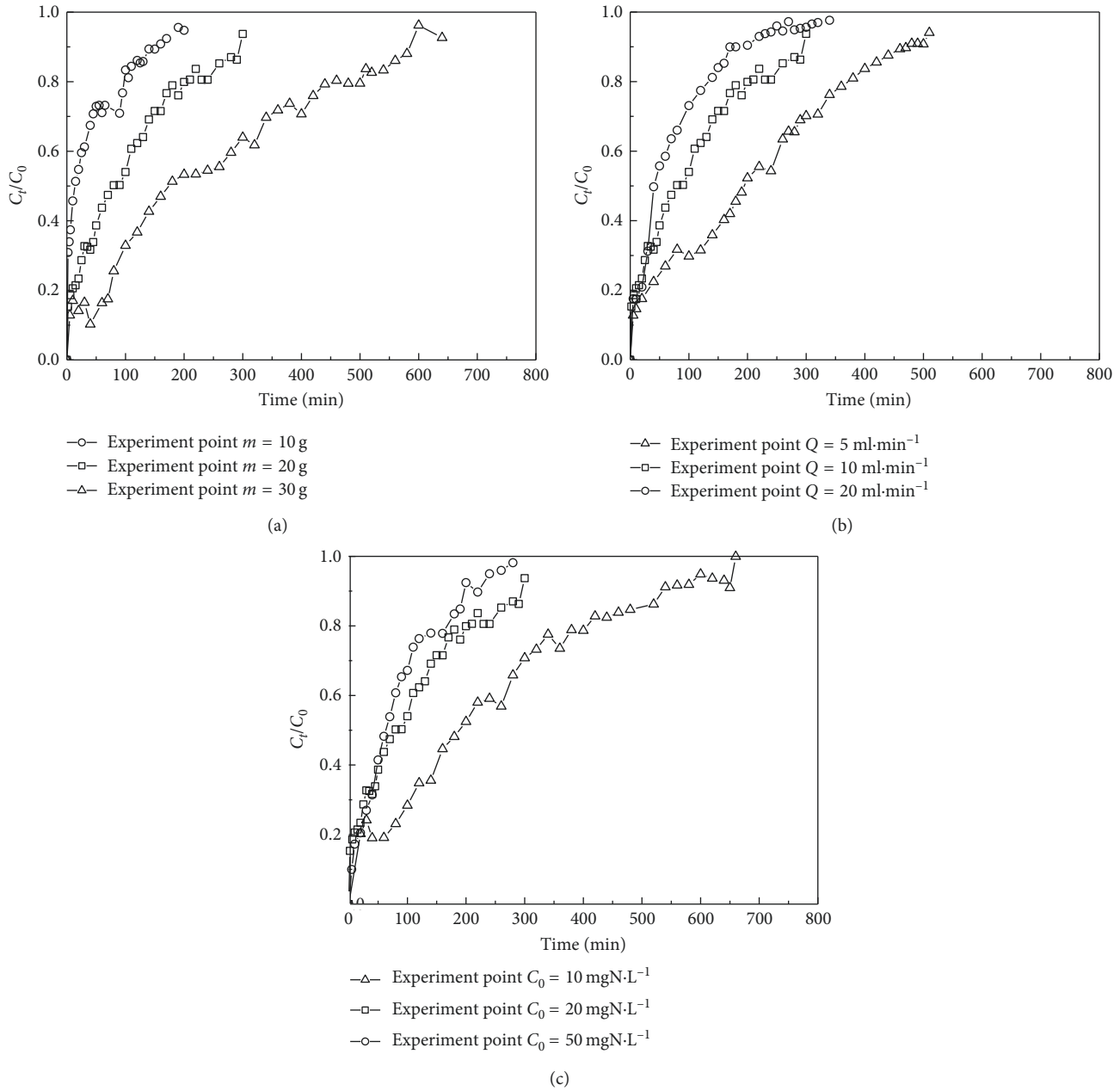

Figure 7: Breakthrough curve: (a) the effect of column depth on NO_3^--N adsorption ($Q = 10$ ml·min^{-1}, $C_0 = 20$ mgN·L^{-1}); (b) the effect of flow rate on NO_3^--N adsorption ($m = 30$ g, $C_0 = 20$ mgN·L^{-1}); (c) the effect of influent concentration on NO_3^--N adsorption ($m = 30$ g, $Q = 10$ ml·min^{-1}).

change of concentration gradient affected the saturation rate and breakthrough time [46, 47].

3.4.4. Application of Thomas Model and Yoon–Nelson Model. Thomas model was widely used to describe the performance of adsorption process in a fixed-bed column. This model assumed plug flow behavior in the bed and used Langmuir isotherm for equilibrium and the second-order reversible kinetics [48]. The model was described by the following equation:

$$\ln\left(\frac{C_0}{C_t} - 1\right) = \frac{K_{th} q_0 m}{Q} - K_{th} C_0 t, \tag{10}$$

where K_{th} (L·min^{-1}·mg^{-1}) is the Thomas rate constant, q_0 (mgN·g^{-1}) is the maximum sorption capacity, m (g) is the mass of adsorbent, and Q (ml·min^{-1}) is the flow rate.

Table 6: Parameters in fixed-bed column for nitrate adsorption by $ZnCl_2$-modified CGAC.

m (g)	Q (ml·min^{-1})	C_0 (mgN·L^{-1})	t_{total} (min)	m_{total} (mg)	q_{total} (mg)	q_{eq} (mgN·g^{-1})	V_{eff} (ml)
10	10	20	200	40.13	2.52	0.25	2000
20	10	20	320	64.21	4.03	0.20	3200
30	10	20	650	133.63	5.05	0.17	6500
20	20	20	290	112.51	5.38	0.27	5800
20	5	20	520	47.82	3.63	0.18	2600
20	10	10	640	65.03	2.31	0.12	6400
20	10	50	260	129.16	5.21	0.26	2600

Table 7: Thomas parameters at different conditions using linear regression analysis.

m (g)	Q (ml·min^{-1})	C_0 (mgN·L^{-1})	K_{Th} (ml·(min·mgN)$^{-1}$) × 10^{-4}	q_0 (mgN·g^{-1})	R^2
10	10	20	22.00	0.24	0.834
20	10	20	6.97	0.94	0.955
30	10	20	3.39	1.55	0.955
20	20	20	12.10	1.15	0.947
20	5	20	4.65	0.94	0.986
20	10	10	7.60	1.06	0.975
20	10	50	4.61	1.79	0.956

Table 8: Yoon–Nelson parameters at different conditions using linear regression analysis.

m (g)	Q (ml·min^{-1})	C_0 (mgN·L^{-1})	K_{YN} × 10^{-2} (min^{-1})	τ (min)	R^2
10	10	20	2.20	24.00	0.833
20	10	20	1.40	93.73	0.955
30	10	20	0.68	232.82	0.955
20	20	20	2.35	59.30	0.947
20	5	20	0.86	203.73	0.986
20	10	10	0.77	208.80	0.975
20	10	50	2.29	72.25	0.956

A simple theoretical model developed by Yoon and Nelson was also tested to investigate the breakthrough behavior of nitrate onto $ZnCl_2$-modified CGAC [49, 50]. The linearized model for a single component system was expressed as follows:

$$\ln\left(\frac{C_t}{C_0 - C_t}\right) = K_{YN}t - \tau K_{YN}, \quad (11)$$

where K_{YN} (min^{-1}) is the rate constant of model and τ (min) is the time required for 50% adsorbate breakthrough.

Among Thomas and Yoon–Nelson models, the parameters listed in Tables 7 and 8, both of them provided good fit ($R^2 > 0.834$) to the experimental data at various conditions. In a comparison of values of R^2 and breakthrough curves, both Thomas and Yoon–Nelson models could be used to describe the behavior of the nitrate adsorption in a fixed-bed column. The results indicated that the external and internal diffusions would not be the limiting step [44].

4. Conclusions

(1) Nitrate adsorption behavior of CGAC and $ZnCl_2$-modified CGAC was described successfully by both Langmuir and Freundlich models, and the maximum adsorption capacity was predicted to be 14.01 mgN·g^{-1} and 0.28 mgN·g^{-1}, respectively. The kinetic data indicated that the adsorption process obeyed the pseudo-second-order model.

(2) The characteristics (SEM and EDAX, surface area, pore structure, zeta potential, Raman spectra, and FTIR) indicated that the mechanism of nitrate adsorption mostly depended on the electrostatic attraction between the free nitrate ions and the positively charged ions, almost without any chemical interactions.

(3) In column study, the breakthrough curves were strongly dependent on the mass of adsorbents, flow rate, and initial NO_3^--N concentration. Both Thomas and Yoon–Nelson models were found to be in good agreement with the experimental data and could be used for prediction of the experimental results as well.

Conflicts of Interest

The authors declare that there are no conflicts of interest regarding the publication of this paper.

Acknowledgments

The research was supported by the National Key Research and Development Program of China (2016YFC0401107) and National Science and Technology Major Project (2015ZX07203-011).

References

[1] N. Ozturk and T. E. Bektas, "Nitrate removal from aqueous solution by adsorption onto various materials," *Journal of Hazardous Materials*, vol. 112, no. 1-2, pp. 155–162, 2004.

[2] L. Kuai and W. Verstraete, "Ammonium removal by the oxygen-limited autotrophic nitrification-denitrification system," *Applied and Environmental Microbiology*, vol. 64, no. 11, pp. 4500–4506, 1998.

[3] Y. H. Huang and T. C. Zhang, "Effects of low pH on nitrate reduction by iron powder," *Water Research*, vol. 38, no. 11, pp. 2631–2642, 2004.

[4] A. Agrawal and P. G. Tratnyek, "Reduction of nitro aromatic compounds by zero-valent iron metal," *Environmental Science and Technology*, vol. 30, no. 1, pp. 153–160, 1995.

[5] B. Ileri, O. Ayyildiz, and O. Apaydin, "Ultrasound-assisted activation of zero-valent magnesium for nitrate denitrification: identification of reaction by-products and pathways," *Journal of Hazardous Materials*, vol. 292, pp. 1–8, 2015.

[6] R. Lucchetti, A. Siciliano, L. Clarizia et al., "Sacrificial photocatalysis: removal of nitrate and hydrogen production by nano-copper-loaded P25 titania. A kinetic and ecotoxicological assessment," *Environmental Science and Pollution Research International*, vol. 24, no. 6, pp. 5898–5907, 2017.

[7] R. Epsztein, O. Nir, O. Lahav, and M. Green, "Selective nitrate removal from groundwater using a hybrid nanofiltration-reverse osmosis filtration scheme," *Chemical Engineering Journal*, vol. 279, pp. 372–378, 2015.

[8] Z. Zhang, Y. Xu, W. Shi et al., "Electrochemical-catalytic reduction of nitrate over Pd–Cu/γAl_2O_3 catalyst in cathode chamber: enhanced removal efficiency and N_2 selectivity," *Chemical Engineering Journal*, vol. 290, pp. 201–208, 2016.

[9] A. M. Bergquist, J. K. Choe, T. J. Strathmann, and C. J. Werth, "Evaluation of a hybrid ion exchange-catalyst treatment technology for nitrate removal from drinking water," *Water Research*, vol. 96, pp. 177–187, 2016.

[10] S. Samatya, N. Kabay, U. Yuksel, M. Arda, and M. Yuksel, "Removal of nitrate from aqueous solution by nitrate selective ion exchange resins," *Reactive and Functional Polymers*, vol. 66, no. 11, pp. 1206–1214, 2006.

[11] D. Ucar, E. U. Cokgor, and E. Sahinkaya, "Evaluation of nitrate and perchlorate reduction using sulfur-based autotrophic and mixotrophic denitrifying processes," *Water Science and Technology-Water Supply*, vol. 16, no. 1, pp. 208–218, 2016.

[12] M. Mazarji, B. Aminzadeh, M. Baghdadi, and A. Bhatnagar, "Removal of nitrate from aqueous solution using modified granular activated carbon," *Journal of Molecular Liquids*, vol. 233, pp. 139–148, 2017.

[13] A. Bhatnagar, M. Ji, Y. Choi et al., "Removal of nitrate from water by adsorption onto zinc chloride treated activated carbon," *Separation Science and Technology*, vol. 43, no. 4, pp. 886–907, 2008.

[14] M. Kalaruban, P. Loganathan, W. G. Shim et al., "Removing nitrate from water using iron-modified Dowex 21K XLT ion exchange resin: batch and fluidised-bed adsorption studies," *Separation and Purification Technology*, vol. 158, pp. 62–70, 2016.

[15] L. D. Hafshejani, A. Hooshmand, A. A. Naseri, A. S. Mohammadi, F. Abbasi, and A. Bhatnagar, "Removal of nitrate from aqueous solution by modified sugarcane bagasse biochar," *Ecological Engineering*, vol. 95, pp. 101–111, 2016.

[16] H. Demiral and G. Gunduzoglu, "Removal of nitrate from aqueous solutions by activated carbon prepared from sugar beet bagasse," *Bioresource Technology*, vol. 101, no. 6, pp. 1675–1680, 2010.

[17] M. Kalaruban, P. Loganathan, W. G. Shim, J. Kandasamy, H. H. Ngo, and S. Vigneswaran, "Enhanced removal of nitrate from water using amine-grafted agricultural wastes," *Science of the Total Environment*, vol. 565, pp. 503–510, 2016.

[18] X. Xu, B. Gao, Q. Yue, Q. Li, and Y. Wang, "Nitrate adsorption by multiple biomaterial based resins: application of pilot-scale and lab-scale products," *Chemical Engineering Journal*, vol. 234, pp. 397–405, 2013.

[19] X. Xu, B. Gao, Y. Zhao et al., "Nitrate removal from aqueous solution by *Arundo donax* L. reed based anion exchange resin," *Journal of Hazardous Materials*, vol. 203-204, pp. 86–92, 2012.

[20] M. Muthu, D. Ramachandran, N. Hasan, M. Jeevanandam, J. Gopal, and S. Chun, "Unprecedented nitrate adsorption efficiency of carbon-silicon nano composites prepared from bamboo leaves," *Materials Chemistry and Physics*, vol. 189, pp. 12–21, 2017.

[21] A. Rajeswari, A. Amalraj, and A. Pius, "Adsorption studies for the removal of nitrate using chitosan/PEG and chitosan/PVA polymer composites," *Journal of Water Process Engineering*, vol. 9, pp. 123–134, 2016.

[22] L. Krayzelova, T. J. Lynn, Q. Banihani, J. Bartacek, P. Jenicek, and S. J. Ergas, "A tire-sulfur hybrid adsorption denitrification (T-SHAD) process for decentralized wastewater treatment," *Water Research*, vol. 61, pp. 191–199, 2014.

[23] Y. Wu, Y. Wang, J. Wang et al., "Nitrate removal from water by new polymeric adsorbent modified with amino and quaternary ammonium groups: batch and column adsorption study," *Journal of the Taiwan Institute of Chemical Engineers*, vol. 66, pp. 191–199, 2016.

[24] W. M. Golie and S. Upadhyayula, "An investigation on biosorption of nitrate from water by chitosan based organic-inorganic hybrid biocomposites," *International Journal of Biological Macromolecules*, vol. 97, pp. 489–502, 2017.

[25] M. Islam and R. Patel, "Nitrate sorption by thermally activated Mg/Al chloride hydrotalcite-like compound," *Journal of Hazardous Materials*, vol. 169, no. 1–3, pp. 524–531, 2009.

[26] V. Alimohammadi, M. Sedighi, and E. Jabbari, "Response surface modeling and optimization of nitrate removal from aqueous solutions using magnetic multi-walled carbon nanotubes," *Journal of Environmental Chemical Engineering*, vol. 4, no. 4, pp. 4525–4535, 2016.

[27] W. Song, B. Gao, X. Xu et al., "Adsorption of nitrate from aqueous solution by magnetic amine-crosslinked biopolymer based corn stalk and its chemical regeneration property," *Journal of Hazardous Materials*, vol. 304, pp. 280–290, 2016.

[28] Z. Ren, X. Xu, X. Wang et al., "FTIR, Raman, and XPS analysis during phosphate, nitrate and Cr(VI) removal by amine cross-linking biosorbent," *Journal of Colloid and Interface Science*, vol. 468, pp. 313–323, 2016.

[29] F. Ogata, D. Imai, and N. Kawasaki, "Adsorption of nitrate and nitrite ions onto carbonaceous material produced from soybean in a binary solution system," *Journal of Environmental Chemical Engineering*, vol. 3, no. 1, pp. 155–161, 2015.

[30] X. Xing, B. Y. Gao, Q. Q. Zhong, Q. Y. Yue, and Q. Li, "Sorption of nitrate onto amine-crosslinked wheat straw: characteristics, column sorption and desorption properties," *Journal of Hazardous Materials*, vol. 186, no. 1, pp. 206–211, 2011.

[31] N. Ozturk and D. Kavak, "Adsorption of boron from aqueous solutions using fly ash: batch and column studies," *Journal of Hazardous Materials*, vol. 127, no. 1–3, pp. 81–88, 2005.

[32] E. Oguz and M. Ersoy, "Removal of Cu^{2+} from aqueous solution by adsorption in a fixed bed column and neural network modelling," *Chemical Engineering Journal*, vol. 164, no. 1, pp. 56–62, 2010.

[33] S. Langergren and B. K. Svenska, "Zur theorie der sogenannten adsorption geloester stoffe," *Veternskapsakad Handlingar*, vol. 24, no. 4, pp. 1–39, 1898.

[34] W. J. Weber and J. C. Morris, "Kinetics of adsorption on carbon from solution," *ASCE Sanitary Engineering Division Journal*, vol. 1, no. 2, pp. 1-2, 1963.

[35] R. Katal, M. S. Baei, H. T. Rahmati, and H. Esfandian, "Kinetic, isotherm and thermodynamic study of nitrate adsorption from aqueous solution using modified rice husk," *Journal of Industrial and Engineering Chemistry*, vol. 18, no. 1, pp. 295–302, 2012.

[36] R. Saad, K. Belkacemi, and S. Hamoudi, "Adsorption of phosphate and nitrate anions on ammonium-functionalized MCM-48: effects of experimental conditions," *Journal of Colloid and Interface Science*, vol. 311, no. 2, pp. 375–381, 2007.

[37] B. H. Hameed, A. T. M. Din, and A. L. Ahmad, "Adsorption of methylene blue onto bamboo-based activated carbon: kinetics and equilibrium studies," *Journal of Hazardous Materials*, vol. 141, no. 3, pp. 819–825, 2007.

[38] V. Ponnusami, S. Vikram, and S. N. Srivastava, "Guava (Psidium guajava) leaf powder: novel adsorbent for removal of methylene blue from aqueous solutions," *Journal of Hazardous Materials*, vol. 152, no. 1, pp. 276–286, 2008.

[39] A. Bhatnagar, E. Kumar, and M. Sillanp, "Nitrate removal from water by nano-alumina: characterization and sorption studies," *Chemical Engineering Journal*, vol. 163, no. 3, pp. 317–323, 2010.

[40] C. Lu and F. Su, "Adsorption of natural organic matter by carbon nanotubes," *Separation and Purification Technology*, vol. 58, no. 1, pp. 113–121, 2007.

[41] V. Gomez-Serrano, J. Pastor-Villegas, A. Perez-Florindo, C. Duran-Valle, and C. Valenzuela-Calahorro, "FT-IR study of rockrose and char and activated carbon," *Journal of Analytical and Applied Pyrolysis*, vol. 36, no. 1, pp. 71–80, 1996.

[42] H. Cavendish and J. Planta, "Adsorption of nitrate and Cr(VI) by cationic polymer-modified granular activated carbon," *Chemical Engineering Journal*, vol. 175, no. 1, pp. 298–305, 2011.

[43] S. Chen, Q. Yue, B. Gao, Q. Li, X. Xu, and K. Fu, "Adsorption of hexavalent chromium from aqueous solution by modified corn stalk: a fixed-bed column study," *Bioresource Technology*, vol. 113, pp. 114–120, 2012.

[44] R. Han, Y. Wang, X. Zhao et al., "Adsorption of methylene blue by phoenix tree leaf powder in a fixed-bed column: experiments and prediction of breakthrough curves," *Desalination*, vol. 245, no. 1–3, pp. 284–297, 2009.

[45] S. S. Baral, N. Das, T. S. Ramulu, S. K. Sahoo, S. N. Das, and G. R. Chaudhury, "Removal of Cr(VI) by thermally activated weed Salvinia cucullata in a fixed-bed column," *Journal of Hazardous Materials*, vol. 161, no. 2-3, pp. 1427–1435, 2009.

[46] R. Han, Y. Wang, W. Zou, Y. Wang, and J. Shi, "Comparison of linear and nonlinear analysis in estimating the Thomas model parameters for methylene blue adsorption onto natural zeolite in fixed-bed column," *Journal of Hazardous Materials*, vol. 145, no. 1-2, pp. 331–335, 2007.

[47] J. Goel, K. Kadirvelu, C. Rajagopal, and V. Kumar Garg, "Removal of lead(II) by adsorption using treated granular activated carbon: batch and column studies," *Journal of Hazardous Materials*, vol. 125, no. 1–3, pp. 211–220, 2005.

[48] N. Rahman and M. F. Khan, "Nitrate removal using poly-o-toluidine zirconium(IV) ethylenediamine as adsorbent: batch and fixed-bed column adsorption modelling," *Journal of Water Process Engineering*, vol. 9, pp. 254–266, 2016.

[49] K. S. Rao, S. Anand, and P. Venkateswarlu, "Modeling the kinetics of Cd(II) adsorption on *Syzygium cumini* L leaf powder in a fixed bed mini column," *Journal of Industrial and Engineering Chemistry*, vol. 17, no. 2, pp. 174–181, 2011.

[50] Y. H. Yoon and J. H. Nelson, "Application of gas adsorption kinetics I. A theoretical model for respirator cartridge service life," *American Industrial Hygiene Association*, vol. 45, no. 8, pp. 509–516, 1984.